Statistical Measures for the Dynamical Atom-Field Coupling Constants [†]

Abu Mohamed Alhasan [‡]

Physics Department, Faculty of Science, Assiut University, Assiut 71516, Egypt; am.alhasan.sq@gmail.com

† Presented at 1st International Electronic Conference on Applied Sciences, 10–30 November 2020;
   Available online: https://asec2020.sciforum.net/.

‡ Current address: Bağlar Mahallesi, 31500 Ryhanlı, Hatay, Turkey.

Abstract: We establish a statistical-measures approach to describe the spectral-spatial analysis of the dynamical atom-field couplings associated with two-pair of pulses propagation in multilevel atomic media. The statistical measures are functional measures that depend on the collective coupling as well as on the eigenvalues of the Nonlinear-Liouville equation. The Nonlinear-Liouville equation is a nonlinear evolution equation which is a second-order differential equation in time. It describes the multi-wave mixing process within the atomic system, as well as coherent oscillations. The proposed spectral estimators prevail spatial multi-peak structure, which depends on the reduction or the enhancement of an effective Rabi-frequency. Decomposition of collective oscillations provides an intuitive guess to special-weight of the field's area. We introduce two functional wavelets to simulate the atomic polarization response. One of these functionals exposes the dependence on the multi-component sine-Gordon equation for the atomic polarization, which is adequate at relatively small propagation distances. The second one is composed of combined sine and cosine functionals on the area of the fields. The cosine functional reflects the significance of the atomic inversion on the polarization response to electromagnetic field excitations. The proposed functional-wavelets inducts new sources for soliton features to the transition-radiation propagation associated with Maxwell-Bloch equations.

Keywords: hyperfine structure; Coupling Constants; spectral estimators; nonlinear-liouville equation; combined sine-cosine-gordon equation

PACS: 02.70.Hm; 31.15.bt; 32.10.Fn; 95.30.Ky; 42.50.p; 42.50.Gy; 42.50.Hz; 42.81.Dp

1. Introduction

Recently, we have introduced a dynamical-graph-model (DGM) to simulate short pulses propagation in multilevel atomic media [1]. However, certain aspects of the propagation dynamics are still unresolved up-to-date. Specifically, the form of the atomic polarization response as the pulse spatially stabilize in its area or energy. The problem is analytically intractable due to the induced multi-wave mixing (MWM) processes associated with strong field excitations [2]. We intend to describe two-pair pulses propagation in gaseous media, such as ^{87}Rb vapors with a nuclear spin 3/2. The excitation dynamics of a four-level atomic media studied in different connections. In the Schrödinger representation, Sharma et al. discussed the temporal behavior of the atomic populations under intense laser fields [3,4]. Gong and Rice discussed a five-level four-pulse extended stimulated Raman adiabatic passage (STIRAP) scheme to control the population transfer branching ratio between two degenerate target states [5]. Hioe et al. investigated the adiabatic solitary-wave solutions of the three- and N-level atomic systems, where several conditions imposed on the interaction

parameters [6,7]. Grigoryan et al. obtained the adiabatic conditions for transparency of short pulses in multilevel atoms using the method of quasi-energies [8]. The coupling constant behavior of eigenvalues of Zakharov-Shabat systems has been reported [9] (and references therein).

2. Theoretical Description

This work presents a theoretically-based model for polychromatic field excitation of multilevel atoms generated by the hyperfine structure (hf). As an example we consider the D_1-line, i.e., the transition $5\,^2S_{1/2} - 5\,^2P_{1/2}$ in ^{87}Rb atoms. The multilevel structure is depicted schematically in Figure 1, with its four-level bare states. The kets $|1\rangle = |5\,^2S_{1/2}, F_1 = 1\rangle$, and $|2\rangle = |5\,^2S_{1/2}, F_2 = 2\rangle$ represent the ground hf states. While $|3\rangle = |5\,^2P_{1/2}, F_3 = 3\rangle$, and $|4\rangle = |5\,^2P_{1/2}, F_4 = 2\rangle$ denote the excited hf states. The number F_α denotes the total angular momentum quantum number associated with hf level with a level index α, and $\alpha = 1, \dots, 4$. The fields with Rabi frequencies Ω_{13}, and Ω_{14} are tuned to the optical transitions $1 \leftrightarrow 3$, and $1 \leftrightarrow 4$, respectively. In addition, the fields with Rabi frequencies Ω_{23}, and Ω_{24} connect the transitions $2 \leftrightarrow 3$ and $2 \leftrightarrow 4$, respectively.
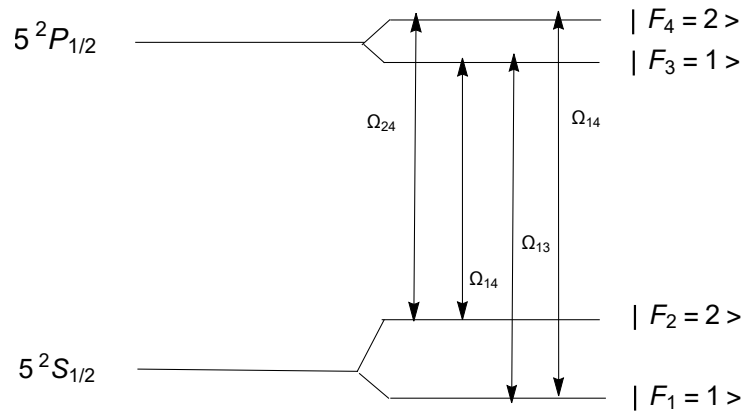
Figure 1. Energy level diagram of ^{87}Rb D_1-line including hyperfine structure. The Rabi frequencies Ω_{ij} couple the dipole allowed transition $|F_i\rangle \Leftrightarrow |F_j\rangle$, where i and j denote the level label with $i = \{3, 4\}$, and $j = \{1, 2\}$, respectively.

The state of the dressed atom is described by the Liouville-von Neumann type equation (LvNME) for the reduced density operator in the Liouvillan product space [10]. We have developed Fiutak and van Kranendonk approach for fine structure interaction of light with matter [11] to hyperfine structure interaction. Following our previous papers, we shall work using relative units. The relative retarded time in a frame moving with pulse is $\tau = \gamma(t - z/c)$. The dimensionless spatial variable is given as $\zeta = \alpha'(z + ct)$. Where t is the time, c is the velocity of light, z is the spatial variable, and α' is the absorption coefficient of one of the pulses at the injection point [12]. The atom-field coupling v is defined as $v = \frac{d_r E}{2\sqrt{3}\hbar}$, where d_r is the reduced dipole moment of the optical transition and E is the electric field amplitude. The Rabi frequency is related to atom-field coupling by the relation: $\Omega = \sqrt{8}v$. The relative atom-field coupling becomes $\mathsf{v} = v/\gamma$, and γ is the spontaneous decay rate of the atomic excited state $P_{1/2}$. The Rabi frequency is related to the light intensity I and the saturation intensity I_{sat} by $I/I_{sat} = 2\Omega^2/\gamma^2$ equality [13]. We have 28 density matrix components (DMC) $\rho_{\alpha\beta}^{(Fm)}$ associated with the D_1-line taking into account the hf structure. The labels α and β take values from 1 to 4. The labels F and m denote the tensor rank, and the magnetic quantum number, respectively. The DMC are normalized subjected to the trace metric condition $\text{Tr}\rho = \sqrt{3}\rho_{11}^{(00)} + \sqrt{5}\rho_{22}^{(00)} + \sqrt{3}\rho_{33}^{(00)} + \sqrt{5}\rho_{44}^{(00)} = 1$. Let us briefly mention the relevant DMC. There are four components of rank zero, $\{\rho_{11}^{(00)}, \rho_{22}^{(00)}, \rho_{33}^{(00)}, \rho_{44}^{(00)}\}$, which are proportional to the atomic level populations. The components with a first rank, $\{\rho_{31}^{(10)}, \rho_{41}^{(10)}, \rho_{32}^{(10)}, \rho_{42}^{(10)}\}$,

refer to the atomic coherence. The components, $\{\rho_{21}^{(20)}, \rho_{43}^{(20)}\}$, represent the lower and upper Raman coherence, respectively. The components, $\{\rho_{11}^{(20)}, \rho_{22}^{(20)}, \rho_{33}^{(20)}, \rho_{44}^{(20)}\}$, represent the alignment of the four-hf states. There are three components of the third rank, $\{\rho_{42}^{(30)}, \rho_{32}^{(30)}, \rho_{41}^{(30)}\}$. These elements correspond to the correlations between the upper (3,4) and lower (2,1) hf levels. Finally, we have the hexadecapole components for the fourth and second hf levels as $\rho_{44}^{(40)}$, and $\rho_{22}^{(40)}$, respectively. The magnetic quantum number $m = 0$, as we consider linear polarization. We are interested in the resonant pulse propagation. Therefore, lower hf splitting, $\Delta\omega_{21}$, is compensated by the frequency difference between the fields Ω_{31} and Ω_{32}. The upper hf splitting, $\Delta\omega_{43}$, is compensated by the frequency difference between the fields with Rabi frequencies Ω_{42} and Ω_{32}. The two two-photon in resonance conditions will enable us to maintain a well-defined area for the field's envelope, as we have zero initial phases. We shall assume a t^2-Gaussian shape for the injected pulse's envelope in the form $v(t) = 64\sqrt{2\pi}v_0/27(t/T_p)^2 \exp[-8/9\pi(t/T_p)^2]$, where v_0 is the mean amplitude of the pulse, and T_p its time duration. The time evolution of the DMC is listed in [10]. The reduced Maxwell-field equations in a frame moving with the pulse can be written as:

$$\partial v_{13}(\zeta,\tau)/\partial\zeta = -\rho_{13}^{(10)}(\zeta,\tau), \quad \partial v_{14}(\zeta,\tau)/\partial\zeta = \rho_{14}^{(10)}(\zeta,\tau),$$
$$\partial v_{23}(\zeta,\tau)/\partial\zeta = -\rho_{23}^{(10)}(\zeta,\tau), \quad \partial v_{24}(\zeta,\tau)/\partial\zeta = \rho_{24}^{(10)}(\zeta,\tau). \tag{1}$$

In the following, we describe the atom-field coupling associated with the multilevel system considered.

3. The Effective Statistical-Weight for Dynamical Atom-Field Coupling in Two Pair Pulses Propagation

The Maxwell-Bloch (MB) equations describe the dynamics of two-pair of pulses propagation [10]. We shall write these equations in matrix form as

$$\partial_t Y(z,t) = L(\tilde{v}(z,t))Y(z,t), \tag{2}$$

where $\tilde{v}(z,t) = \{v_{13}(z,t), v_{14}(z,t), v_{23}(z,t), v_{24}(z,t)\}$ stands for atom-field couplings associated with the double-Λ system. The components of $Y(z,t)$ at fixed spatial point are the DMC of the type $\rho_{\alpha\beta}^{(F)}$ where F denotes the rank of the tensor. The matrix $L(\tilde{v}(z,t))$ stands for the matrix of coefficients. Equation (1) presents the reduced Maxwell-field equations. The system Equations (1) and (2) forms the reduced Maxwell-Bloch equations (RMB). We can arrange the second-order derivative of $Y(z,t)$ w.r.t time to be the Nonlinear-Liouville equation (NLLE) as

$$\partial_{tt}^2 Y(z,t) = \mathcal{M}(\gamma v_\alpha(z,t), v_\alpha(t)v_\beta(z,t), \partial_t v_\alpha(z,t))Y(z,t), \tag{3}$$

and $\mathcal{M}$ is the coefficient matrix of $\rho_{\alpha\beta}^{(k)}(t)$ in $Y(z,t)$. The matrix $\mathcal{M}$ depends on the fields, and its first derivative w.r.t time as well as two-wave mixing. Let us establish the first-rank coherence-tensor $X^{(1m)}(t)$. It comprises of the components $\rho_{13}^{(1m)}(t), \rho_{14}^{(1m)}(t), \rho_{23}^{(1m)}(t)$, and $\rho_{24}^{(1m)}(t)$. The coherence-tensor can be written as

$$X^{(1m)}(t) = (\rho_{13}^{(1m)}(t) \ \rho_{14}^{(1m)}(t) \ \rho_{23}^{(1m)}(t) \ \rho_{24}^{(1m)}(t))^{\mathrm{T}}, \tag{4}$$

where T denotes here the transpose. Let us consider the case of constant couplings in space and time. The second-derivative of the coherence tensor becomes

$$\partial_{tt}^2 X^{(1m)}(t) = \Omega(\tilde{v}) X^{(1m)}(t), \tag{5}$$

and $\Omega(\tilde{v})$ is the MWM tensor.

The time evolution of the coherence-tensor is influenced by the storage-tensor components, which acts as a source terms in the time development of the coherence-tensor. Free dipole oscillations are

obtained when both longitudinal and transverse relaxation rates vanished, i.e., $\gamma = 0$, and $\Gamma = 0$. In deriving the second-derivative of the coherence-tensor, we shall ignore contributions from Raman coherence and dissipative second-rank tensors $\rho_{\alpha\beta}^{(20)}$. Additionally, we ignore contributions from third- and, fourth-rank tensors. The influence of these elements is treated subsequently. The elements of the MWM tensor $\Omega(\tilde{v})$ are quadratic in Rabi frequencies. Since it contains the products $v_\alpha v_\beta$. The diagonal matrix elements of $\Omega(\tilde{v})$ are composed from summation over quadratic terms as $\sum_\alpha v_\alpha^2$. While off diagonal matrix elements contain the MWM, i.e., terms like $\sum_{\alpha,\beta} v_\alpha v_\beta$, where $\alpha \neq \beta$. It is difficult to find eigenvalues of the MWM matrix for $\Omega(\tilde{v})$. Therefore, it is instructive to consider the case when all the frequencies are equal in which $v_\alpha = v$. In this special case, the coefficient matrix contains one factor, simply v^2 and can be diagonalized. The eigenvalues of the MWM matrix are

$$\lambda = \left\{ -8v^2, -8v^2, -8v^2, -\frac{16v^2}{5} \right\}. \tag{6}$$

We have obtained two distinct definitions for the statistical-weight of the pulse's area as

$$\kappa = \left\{ \sqrt{8}, \frac{4}{\sqrt{5}} \right\}. \tag{7}$$

The justification of these values will be tested across propagation and stabilization of the area, as we did in our earlier work [10]. Thus, it is possible to assign $-\lambda/v^2$ to the statistical-weight of the energy of the pulse in the presence of relaxations and whenever we have real eigenvalues, as the singular-value decomposition technique is adopted. Then, the effective measure for the statistical-weight for the pulse's area can be written as

$$\kappa_{eff}(\zeta) = \ \ [\lambda(\zeta)/v^2(\zeta)]^{1/2}. \tag{8}$$

We emphasize that the definition of $\kappa_{eff}(\zeta)$ may generalize the atom-field coupling constant concept to one which depends on the atomic relaxations. In fact, the atom-field coupling is a static property while $\kappa_{eff}(\zeta)$ is a dynamic coupling. The dynamic coupling reflects the influences of the pulse shape, and its time-derivative as well as the atomic relaxations. The foregoing analysis shows that the fundamental frequency λ_1, that has the biggest real eigenvalue, predicts the presumed statistical-weight for the area of the fields at $z = 0$. That is, where the fields are equally, initially. This means that

$$\frac{\lambda_1}{8v^2} = 1. \tag{9}$$

Thereafter, Equation (9) defines an effective Rabi frequency for the system of double-Λ excitation. This is in agreement with our previous result $\Omega(\zeta,\tau) = \kappa v(\zeta,\tau)$, and $\kappa = \sqrt{8}$, presented in [10]. However, we have found that it is true only for stable area propagation and for one transition only, that is $|F_1 = 1\rangle \leftrightarrow |F_3 = 2\rangle$ transition.

We define the spatial mean-coupling associated with each pulse corresponding to its optical transition as

$$v_\alpha(z) = \frac{\int v_\alpha(z,t)^2 dt}{\int v_\alpha(z,t) dt}. \tag{10}$$

The mean-energy for each pulse is given by $v_\alpha^2(z)$. Therefore, the reduced mean-energy at a given spatial point z is given as

$$\Omega^r(z) = v_{eq}^2(z) = v_{13}^2(z) + 5[v_{14}^2(z) + v_{23}^2(z) + v_{24}^2(z)], \tag{11}$$

for the composed system. Consequently, we can define a spatial functional-measure concerning dynamical statistical-weight of the pulse's area as the following

$$K_{\lambda_{max}}(z) = \left[\frac{\max_t \lambda(z,t)}{v_{eq}^2(z)}\right]^{1/2}, \tag{12}$$

and $\lambda(z,t)$ represent the eigenvalues of the matrix $\mathcal{M}$. In general, well shall use the singular-value decomposition technique to obtain the eigenvalues $\lambda(z,t)$. The maximum value is running over the distribution of eigenvalues along time, which guarantees a single value at any spatial point z. The flatten tensor $Y(z,t)$ is composed of 19 components, as we have considered resonant pulses propagation and the fields are assumed to be initially real. The singular-value decomposition technique provides us with the maximum eigenvalue at any instant as the first eigenvalue. The spatial statistical-weight of the area of the collective fields then becomes

$$\kappa(z) = K_{\lambda_{max}}(z). \tag{13}$$

On an energy-based perspective, the spectral estimates $K_\lambda(\zeta)$ are presented in Figure 2 for different eigenvalues in the course of propagation. The spectral estimates associated with the fundamental eigenvalue expose finite sharp peaks in the course of propagation. The peaks correspond to the reduction and the enhancement of the mean-field energy of the composed system. Both reduction and enhancement of the mean-field energy contribute to formation of peaks. The spectral estimators $K_{\lambda_{16}}(\zeta)$ up to $K_{\lambda_{19}}(\zeta)$ are small, and not shown. The radiation transitions may enhance the interference through terms like $v_\alpha(\zeta,\tau)v_\beta(\zeta,\tau)$. The spectral estimators $K_\lambda(0)$ at the injection point display values close to unity for the first ten eigenvalues. It is in consequence of our analytical results presented in Equation (9). The peak structure is smeared for small eigenvalue measures, such as $K_{\lambda_{15}}(\zeta)$. The reduction of effective Rabi frequency, $v_{eq}(\zeta)$, does not completely control the behavior of the functional measures. Therefore, it is instructive to deal with other measures which reflects the statistics of the temporal distribution of eigenvalues. It is to be noted throughout the formalism we use the spatial-temporal point representation (z,t). For numerical illustrations we use (ζ,τ) instead. Let us turn to other functional measures. The second functional-measure is based upon the standard deviation of the temporal eigenvalues as

$$K_\lambda^{(s)}(z) = \left[\frac{\mathrm{SD}_\tau(\lambda(z,t))}{v_{eq}^2(z)}\right]^{1/2}, \tag{14}$$

and SD_τ stands for the standard deviation of eigenvalues w.r.t times and at a given spatial point. The third functional measure is based upon the standard deviation of the auto-correlation function on the temporal eigenvalues at a given spatial point as

$$K_\lambda^{(sc)}(z) = \left[\frac{\mathrm{SD}_t[\mathrm{corr}_t(\lambda(z,t))]^{1/2}}{v_{eq}^2(z)}\right]^{1/2}, \tag{15}$$

and corr_t stands for the auto-correlation function on the temporal eigenvalues. Figure 3 shows comparison between the absorption peaks for different measures. Among these measures, only the $K_1(\zeta)$ measure matches the unity requirement at the injection point $\zeta = 0$ for the fundamental frequency. The increase of $K^{(s)}(\zeta)$ and $K^{(sc)}(\zeta)$ with distances indicate that the temporal eigenvalues are distributed over a wider range of values. This increase of $K^{(sc)}(\zeta)$ in the course of propagation is continued with a little drop as the double-Λ system is collapsed into an upper V_2 subsystem containing the hyperfine states $|F_2 = 2\rangle$, $|F_3 = 1\rangle$, and $|F_4 = 2\rangle$. The measure $K^{(sc)}(\zeta)$ reflects more spreading of eigenvalues about its mean, since $K^{(sc)}(\zeta) > K^{(s)}(\zeta)$.
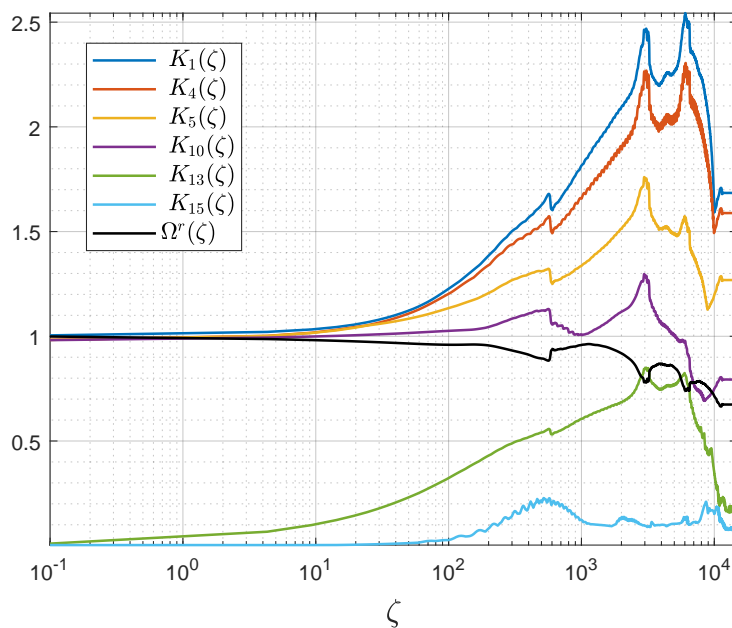
Figure 2. Spectral dependence of the effective statistical-weight for dynamical atom-field coupling on eigenvalues in the course of propagation. The black line presents the reduced mean-energy of the compound system $\Omega^r(\zeta) = v_{eq}^2(\zeta)$ at spatial point ζ.
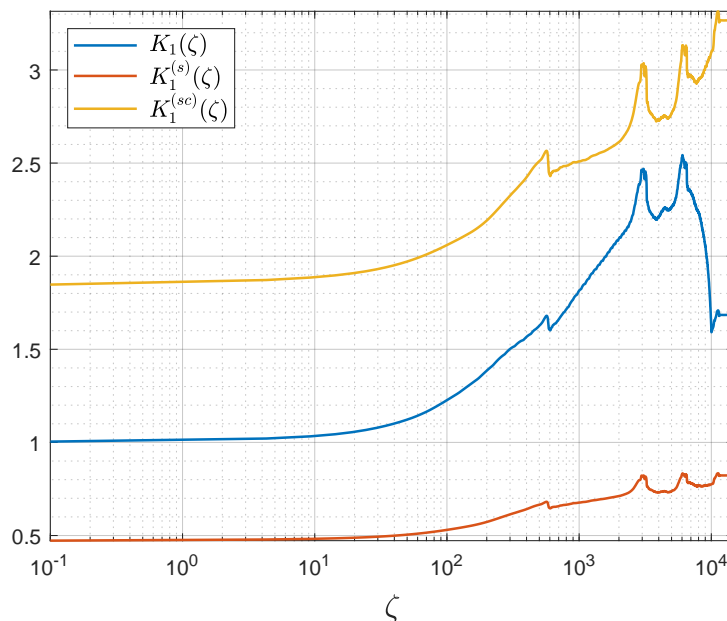
Figure 3. Spatial dependence of the effective statistical-weight for dynamical atom-field coupling. Three different statistics on eigenvalues are shown depending on the maximum eigenvalue $K_1(\zeta)$, the standard deviation of the distribution of eigenvalues $K_1^{(s)}(\zeta)$, and the auto-correlation function $K_1^{(sc)}(\zeta)$, respectively.

4. Multimodal Functional Optimization of the Atomic Polarization

The dynamics of coherent excitation of the two-level atom is inevitably connected to the sine-Gordon (SG) equation [14] (and references therein). The SG equation relates the polarization response of the atomic medium to the electromagnetic field excitation. In this paper, we propose a damped sine-Gordon equation for the atomic polarization as Trρ is conserved, and Tr$\rho^2 \leq 1$. Recently, we analyzed the propagation of short optical pulses [10]. The soliton-like behavior at a stable

positions of the area was discussed. Additionally, the subdivision of the total Bloch vector into its four two-level atoms (TLA) components also demonstrated. In Section 3, we have presented the spectral analysis of the atom-field couplings in the course of propagation. Therefore, we may extend the issue of SG equation to the case of multilevel atoms. Especially, at least near the injection point $\zeta = 0$. We can proceed further to express the atomic response in terms of sine and cosine functionals on dynamical couplings. We attempt in this section to describe the spatial dependence of the polarization amplitude for each TLA in the compound system. Thus, our optimizing procedure accounts for the calculation of a space-dependent polarization amplitude multiplied by a trigonometric functional on the optimized pulse's area. In our study, we solve the initial-value problem of Bloch equations as the atoms are initially at the first hyperfine level, i.e., $n_1(0,0) = 1$. The four exciting fields $v_\alpha(0, \tau)$ have the same mean-amplitude v_0, and mean-duration T_p. We attempt to study short pulses propagation in which $\gamma T_p = 0.1$. Which ensures that the upper hf splitting is well-resolved. Moreover, the pulses have the same area as $\theta_\alpha(0) = 7.8\pi$. It is instructive to look for the atomic coherence in terms of damped SG equation as the field stabilizes in the course of propagation

$$\rho_{14}^{(1m)}(\zeta, \tau) \approx x_1(\zeta) \, \exp(-\Gamma\tau) \sin(x_2(\zeta) \, \vartheta_{14}(\zeta, \tau)), \tag{16}$$

where the time-dependent field area $\vartheta_{14}(\zeta, \tau)$ up to a time τ is given by

$$\vartheta_\alpha(\zeta, \tau) = \sqrt{8} \int_{t_0}^{\tau} v_\alpha(\zeta, \tau')d\tau'. \tag{17}$$

Let $X^{(d)}(\zeta) = [x_1(\zeta), x_2(\zeta), ..., x_d(\zeta)]$ denote the estimate coefficients with dimension d, and $\epsilon^{(d)}(\zeta)$ denotes the squared 2-norm value of the residuals at the spatial point ζ. At $\zeta = 0$, we obtained two parameter estimation values and error as

$$\begin{aligned} X^{(2)}(0) &= [x_1, x_2], \\ &= [-0.2635, 1.0006], \\ \epsilon^{(2)}(0) &= 0.0019. \end{aligned} \tag{18}$$

Figure 4 presents a comparison between the numerical coherence $\rho_{14}^{(10)}(t)$, and the predicted one $\rho_{14}^{(p)}(t)$, as estimated by Equation (16) with two optimization coefficients. We can improve our optimization utilizing the target function as composed of two different trigonometric functionals with different weighting parameters

$$\begin{aligned} \rho_{14}^{(1m)}(\zeta; \tau) \approx &x_1(\zeta) \, \exp(-\Gamma\tau) \sin(x_2(\zeta) \, \vartheta_{14}(\zeta, \tau)) + \\ &x_3(\zeta) \, \exp(-\Gamma\tau) \cos(x_4(\zeta) \, \vartheta_{14}(\zeta, \tau)) - x_3(\zeta) \end{aligned} \tag{19}$$

The approximation presented by Equation (19) gives the weight parameters and the residual sum of squares (RSS) as

$$\begin{aligned} X^{(4)}(0) &= [-0.2646, 1.0002, 0.0017, 0.9387], \\ \epsilon^{(4)}(0) &= 4.910^{-4}. \end{aligned} \tag{20}$$

Figure 5 characterizes the atomic coherence corresponding to $1 \leftrightarrow 4$ transition through the two pair pulses interaction with the four-level atom and exposing four peaks, which signifies the 8π excitation. The vector $X(z)$ reflects the space-dependent amplitude of the atomic polarization corresponding to that transition. It is instructive to maintain contributions of other dipoles on the one understudy. Therefore, we may write the optimizing modal functional as

$$pr(\zeta, \tau) = x_1(\zeta)\sin(x_2(\zeta)\vartheta_2(\zeta, \tau)) + x_3(\zeta)\sin(x_4(\zeta)\vartheta_1(\zeta, \tau)) +$$
$$x_5(\zeta)\sin(x_6(\zeta)\vartheta_3(\zeta, \tau)) + x_7(\zeta)\sin(x_8(\zeta)\vartheta_4(\zeta, \tau)) +$$
$$x_9(\zeta)\cos(x_{10}(\zeta)\vartheta_2(\zeta, \tau)) - x_9(\zeta) + x_{11}(\zeta)\cos(x_{12}(\zeta)\vartheta_1(\zeta, \tau)) - x_{11}(\zeta) +$$
$$x_{13}(\zeta)\cos(x_{14}(\zeta)\vartheta_3(\zeta, \tau)) - x_{13}(\zeta) + x_{15}(\zeta)\cos(x_{16}(\zeta)\vartheta_4(\zeta, \tau)) - x_{15}(\zeta) \tag{21}$$

At the stable area position such as $\zeta = 404$ where the area of the propagated pulses takes the values $\theta_\alpha(\zeta) = [6.5463, 8.0130, 8.8201, 5.5419]$ in π units. The coefficients and error difference between the predicted values according to the modal functional and the numerical values are

$$X^{(16)}(404) = [-0.1973, 0.9828, -0.0700, 1.0858, -0.0667, 0.8221, 0.0679, 1.0534,$$
$$-0.0084, 1.6820, 0.0678, 1.0471, -0.0945, 0.8887, 0.0328, 1.0444], \tag{22}$$
$$\epsilon^{(16)}(404) = 0.0134.$$
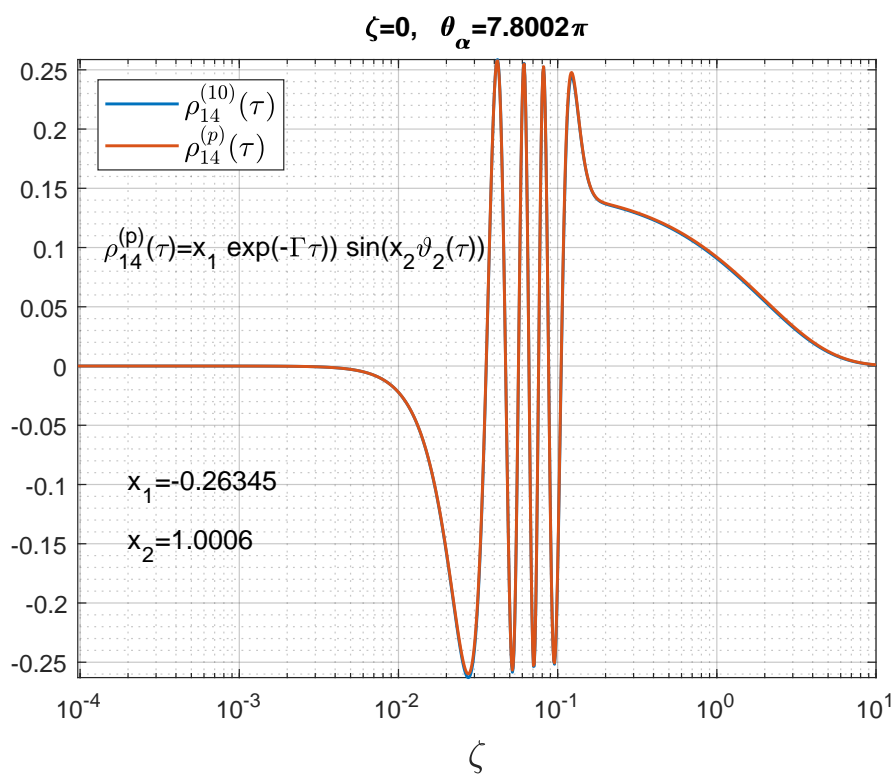
Figure 4. The temporal dependence of the atomic coherence for both numerical $\rho_{14}^{(10)}(\tau)$, and predicted $\rho_{14}^{(p)}(\tau)$ component at the spatial point $\zeta = 0$.

We can decrease the RSS value in using the modal functional as spline functions defined on four-time sections, as an example. The maximum RSS arises in our modal functional for simulation large time behavior, where the predicted modal functional exposes maximum of interference between dipoles. It is to be noted that $X_{even} = [0.9828, 1.0858, 0.8221, 1.0534, 1.6820, 1.0471, 0.8887, 1.0444]$ distributed around unity which shows the statistical-weight of the area is close $\sqrt{8}$. In addition X_{odd} shows negative values for the starting amplitude which characterizes the absorption for small times and preserves the symmetry through the prolonged distance. The study of functional fields [15] due to all-optical transitions is of great importance for understanding the local stability of soliton-like solutions of RMB equations. Our study explores practically the "modal superposition principle" [16] in terms of functionals.
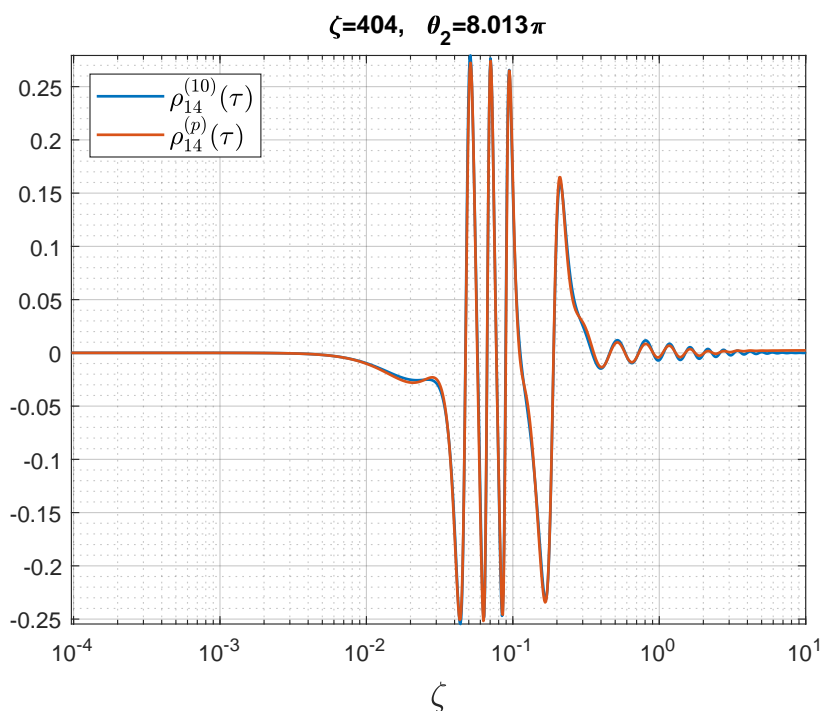
Figure 5. The temporal dependence of the atomic coherence for both numerical $\rho_{14}^{(10)}(\tau)$ and predicted $\rho_{14}^{(p)}(\tau)$ component at the spatial point $\zeta = 404$.

5. Discussions

We have facilitated an energy-based estimation framework to obtain spectral dependence of the dynamical atom-field coupling associated with short pulses propagation in multilevel atomic media. Therefore, we introduced a nonlinear evolution equation, such as the nonlinear-Liouville equation (NLLEQ). It describes the evolution of the mutual interference resulting from frequency-mixing of the transition-radiations along different pathways. Moreover, it involves the amplitude of the energy of the fields, directly, and without the inclusion of Maxwell-fields equations. The proposed estimators are functionals on the pulses mean energy and the relevant eigenvalues of the NLLEQ. The spectral analysis of these estimators shows multiple peaks. The structure of the peaks are devoted to the reduction and enhancement of the pulses mean energy. The polarization responds spatiotemporally through amplitude and frequency modulations of functionals on the area of the fields. Near to the injection point of pulses into the medium, we have shown that the optimized polarization displays uni-modal functional on the field's area associated with optical transitions $1 \leftrightarrow 4$. The uni-modal functional displays the sine-Gordon equation for the atomic polarization. The impact of neighboring transitions on the target polarization are significant for other transitions that is not connected with the ground hf level where the population is assumed to be unity, initially. Therefore, we may expect that the atomic polarization displays multimodal functionals in the form of multi-component sine-Gordon equation corresponding to the relevant optical dipoles. At locally stable positions of the pulse area, the multimodal polarization shows the relevance of multi-component sine- and cosine-Gordon equation with appropriate space-dependent constant to ensure preserving the initial condition. We have considered these functionals as wavelets. The presence of cosine functional in wavelets reflects the impact of the atomic inversion on the optimization of the multimodal polarization.

Conflicts of Interest: "The author declare no conflict of interest".

Abbreviations

The following abbreviations are used in this manuscript:

MDPI	Multidisciplinary Digital Publishing Institute	SG	Sine-Gordon Equation
LvNME	Liouville-von Neumann equation	RMB	Reduced Maxwell-Bloch
NLLE	Nonlinear-Liouville	HF	Hyperfine structure
DGM	Dynamical-graph-model	DMC	Density matrix components
MWM	Multi-wave mixing	RSS	Residual sum of squares

References

1. Alhasan, A.M. Graph Entropy Associated with Multilevel Atomic Excitation. *Proceedings* **2020**, *46*, 9, doi:10.3390/ecea-5-06675.
2. Zhang, Y.; Wen, F.; Xiao, M. *Quantum Control of Multi-Wave Mixing*; Wiley-VCH, Higher Education Press: Weinheim, Germany, 2013.
3. Sharma, M.P.; Roversi, J.A. Dynamics of population of a four-level atom due to one-and three-photon processes. *Phys Rev A* **1984**, *29*, 3264, doi:10.1103/PhysRevA.29.3264.
4. Kancheva, L.; Rashev, S.; Panajotov, K. Remarks on Dynamics of population of a four-level atom due to one-and three-photon processes. *Phys. Rev. A* **1988**, *37*, 4989, doi:10.1103/PhysRevA.37.4989.
5. Gong J.; Rice, S.A. Complete Quantum Control of the Population Transfer Branching Ratio Between Two Degenerate Target States. *J. Chem. Phys.* **2004**, *121*, 1364, doi:10.1063/1.1764503.
6. Hioe, F.T. Adiabatic shape preservation and solitary waves in a five-level atomic medium. *Phys Rev A* **2008**, *78*, 063807, doi:10.1103/PhysRevA.78.063807.
7. Hioe, F.T. Lossless propagation of optical pulses through N-level systems with Gell-Mann symmetry. *J. Opt. Soc. Am. B* **1989**, *6*, 1245–1252, doi:10.1364/JOSAB.6.000335.
8. Grigoryan, G.; Gazazyan, E.; Chaltykyan, V.; Tikhova, O. Adiabatic control of atomic population and distortion-free propagation of short laser pulses in multilevel media. *Laser Phys.* **2014**, *24*, 035301.
9. Klaus, M.; Mityagin. B. Coupling constant behavior of eigenvalues of Zakharov-Shabat systems. *J. Math. Phys.* **2007**, *48*, 123502, doi:10.1063/1.2815810.
10. Alhasan, A.M. Entropy Associated with Local Stabilization of the Pulse Area in Multilevel Atomic Media. *Act. Phys. Poln. A* **2018**, *133*, doi:10.12693/APhysPolA.133.1205.
11. Fiutak, J.; van Kranendonk, J. The effect of collisions on resonance fluorescence and Rayleigh scattering at high intensities. *J. Phys. B At. Mol. Phys.* **1980**, *13*, 2869–2884, doi:10.1088/0022-3700/13/15/006.
12. Horsley, A. High Resolution Field Imaging with Atomic Vapor Cells. Ph.D. Thesis, University of Basel, Basel, Switzerland, 2015
13. Natarajan. V. *Modern Atomic Physics*; CRC Press: Boca Raton, FL, USA, 2015.
14. Alhasan, A.M.; Fiutak, J.; Miklaszewski, W. The influence of the atomic relaxation on the resonant propagation of short light pulses. *Z. Phys. B Condens. Matter* **1992**, *88*, 349–358, doi:10.1007/BF01470924.
15. Volterra, V. *Theory of Functionals and of Integral and Integro-Differential Equations*; Dover Publications: New York, NY, USA, 1959.
16. Fabre, C.; Treps, N. Modes and states in quantum optics. *Rev. Mod. Phys.* **2020**, *92*, 035005, doi:10.1103/RevModPhys.92.035005.

Publisher's Note: MDPI stays neutral with regard to jurisdictional claims in published maps and institutional affiliations.